AMERICAN SOCIETY FOR MICROBIOLOGY | mBio®

RESEARCH ARTICLE

Genome-Wide Characterization of SARS-CoV-2 Cytopathogenic Proteins in the Search of Antiviral Targets

Jiantao Zhang,[a,f] Qi Li,[a] Ruth S. Cruz Cosme,[h] Volodymyr Gerzanich,[c,f] Qiyi Tang,[h] J. Marc Simard,[a,c,g] Richard Y. Zhao[a,b,d,e,f]

[a]Department of Pathology, University of Maryland School of Medicine, Baltimore, Maryland, USA
[b]Department of Microbiology and Immunology, University of Maryland School of Medicine, Baltimore, Maryland, USA
[c]Department of Neurosurgery, University of Maryland School of Medicine, Baltimore, Maryland, USA
[d]Institute of Human Virology, University of Maryland School of Medicine, Baltimore, Maryland, USA
[e]Institute of Global Health, University of Maryland School of Medicine, Baltimore, Maryland, USA
[f]Research & Development Service, VA Maryland Health Care System, Baltimore, Maryland, USA
[g]Surgical Care Clinical Center, VA Maryland Health Care System, Baltimore, Maryland, USA
[h]Department of Microbiology, Howard University College of Medicine, Washington, DC, USA

ABSTRACT Therapeutic inhibition of critical viral functions is important for curtailing coronavirus disease 2019 (COVID-19). We sought to identify antiviral targets through the genome-wide characterization of severe acute respiratory syndrome coronavirus 2 (SARS-CoV-2) proteins that are crucial for viral pathogenesis and that cause harmful cytopathogenic effects. All 29 viral proteins were tested in a fission yeast cell-based system using inducible gene expression. Twelve proteins, including eight nonstructural proteins (NSP1, NSP3, NSP4, NSP5, NSP6, NSP13, NSP14, and NSP15) and four accessory proteins (ORF3a, ORF6, ORF7a, and ORF7b), were identified that altered cellular proliferation and integrity and induced cell death. Cell death correlated with the activation of cellular oxidative stress. Of the 12 proteins, ORF3a was chosen for further study in mammalian cells because it plays an important role in viral pathogenesis and its activities are linked to lung tissue damage and a cytokine storm. In human pulmonary and kidney epithelial cells, ORF3a induced cellular oxidative stress associated with apoptosis and necrosis and caused activation of proinflammatory response with production of the cytokines tumor necrosis factor alpha (TNF-α), interleukin-6 (IL-6), and IFN-β1, possibly through the activation of nuclear factor kappa B (NF-κB). To further characterize the mechanism, we tested a natural ORF3a Beta variant, Q57H, and a mutant with deletion of the highly conserved residue, ΔG188. Compared with wild-type ORF3a, the ΔG188 variant yielded more robust activation of cellular oxidative stress, cell death, and innate immune response. Since cellular oxidative stress and inflammation contribute to cell death and tissue damage linked to the severity of COVID-19, our findings suggest that ORF3a is a promising, novel therapeutic target against COVID-19.

IMPORTANCE The ongoing COVID-19 pandemic caused by SARS-CoV-2 has claimed over 5.5 million lives with more than 300 million people infected worldwide. While vaccines are effective, the emergence of new viral variants could jeopardize vaccine protection. Treatment of COVID-19 by antiviral drugs provides an alternative to battle against the disease. The goal of this study was to identify viral therapeutic targets that can be used in antiviral drug discovery. Utilizing a genome-wide functional analysis in a fission yeast cell-based system, we identified 12 viral candidates, including ORF3a, which cause cellular oxidative stress, inflammation, apoptosis, and necrosis that contribute to cytopathogenicity and COVID-19. Our findings indicate that antiviral agents targeting ORF3a could have a great impact on COVID-19.

Editor Diane E. Griffin, Johns Hopkins Bloomberg School of Public Health

Address correspondence to Richard Y. Zhao, rzhao@som.umaryland.edu.

The authors declare no conflict of interest.

This article is a direct contribution from Richard Yuqi Zhao, a Fellow of the American Academy of Microbiology, who arranged for and secured reviews by Howard B. Lieberman, Columbia University, and T.C. Wu, Johns Hopkins University School of Medicine.

Received 26 January 2022
Accepted 28 January 2022
Published 15 February 2022

KEYWORDS SARS-CoV-2, ORF3a, viral therapeutic target, fission yeast, apoptosis and necrosis, oxidative stress, proinflammatory response, *Schizosaccharomyces pombe*

The ongoing pandemic of coronavirus disease 2019 (COVID-19), caused by severe acute respiratory syndrome coronavirus 2 (SARS-CoV-2), is unprecedented in its rapid spread, persistence, and high fatality. Although current vaccines are effective at preventing SARS-CoV-2 infection, breakthrough infections are not uncommon. Moreover, the emergence of new viral variants could undermine the effectiveness of current vaccines, as well as treatments. For example, of three approved monoclonal antibody treatments, only sotrovimab is effective against the Omicron variant (1). Antiviral drugs are an alternative, potentially effective means to treat SARS-CoV-2 infection and curtail COVID-19 disease, but currently such drugs are limited. The discovery of new antiviral agents is hampered by limited knowledge of the pathogenicity of the virus and of which viral protein(s) should be targeted. There is an urgent need to identify the viral proteins that cause harmful cytopathic effects, tissue damage, and cytokine storm, in order to advance the rational design of anti-COVID-19 therapies.

SARS-CoV-2 belongs to sarbecoviruses, a subgenus of the β-coronaviridae family (2). It is one of the 7 human coronaviruses (hCoVs) that cause human diseases that range from the common cold to severe acute respiratory syndrome (SARS) and Middle East respiratory syndrome (MERS). Like other hCoVs, SARS-CoV-2 is an enveloped, positive-sense (+), single-stranded RNA virus with an average genome size of 29.7 kb. Upon viral entry into a host cell, the (+)ssRNA viral genome is released into the cytoplasm where the two overlapping open reading frames 1a and 1b (ORF1a and ORF1b, respectively) are translated to produce two polyproteins, which are further processed by viral proteases to generate a total of 29 SARS-CoV-2 proteins, including 4 structural proteins, namely, spike (S), envelope (E), membrane (M), and nucleocapsid (N); 16 nonstructural proteins (NSP1 to NSP16); and 9 accessory ORFs (3a, 3b, 6, 7a, 7b, 8, 9b, 9c, and 10) (3). Among them, ORF3a, ORF8, ORF9c, and ORF10 are unique to SARS-CoV-2 (4).

We carried out a genome-wide functional screening of SARS-CoV-2 proteins to identify viral targets that can be used for antiviral drug discovery and testing. We reasoned that SARS-CoV-2 protein therapeutic targets (i) should be essential for virus survival, (ii) should contribute to virus pathogenesis, (iii) should confer measurable cytopathic effects that could be used as endpoints for high-throughput drug screening, and (iv) could be either an established or a novel antiviral drug target. We adapted a unique integrated approach, *viz.*, a well-established fission yeast cell-based system to conduct genome-wide and functional analyses of the viral proteins (5, 6), with the goal of identifying proteins that cause harmful cytopathic effects. Fission yeast (*Schizosaccharomyces pombe*) is a haploid single-cell eukaryotic organism that has been used extensively as a model to study human cancer biology (7) and viruses (5, 6, 8, 9). Fission yeast is a well-tested model system for the study of highly conserved cellular activities (10, 11), such as the cytopathic effects caused by viral proteins, including inhibition of cell proliferation, interruption of cell structural integrity, and induction of apoptosis and necrosis (8). Fission yeast cell-based systems also have been shown to be suitable for antiviral drug testing and drug discovery (5, 12).

A total of 29 viral ORFs (4) representing the entire viral genome were cloned into the fission yeast gene expression system (6, 13). The expression of each viral ORF was under the control of an inducible no message in thiamine (*nmt*1) promoter (13), allowing all SARS-CoV-2-specific viral protein effects to be measured specifically by gene induction versus those without gene induction (6, 8). Using this unique integrated strategy, we report the identification of multiple possible viral therapeutic targets with a detailed description, as a proof-of-concept, of ORF3a. We demonstrate the potential of ORF3a to serve as a therapeutic target for the discovery and testing of antiviral drugs against COVID-19.

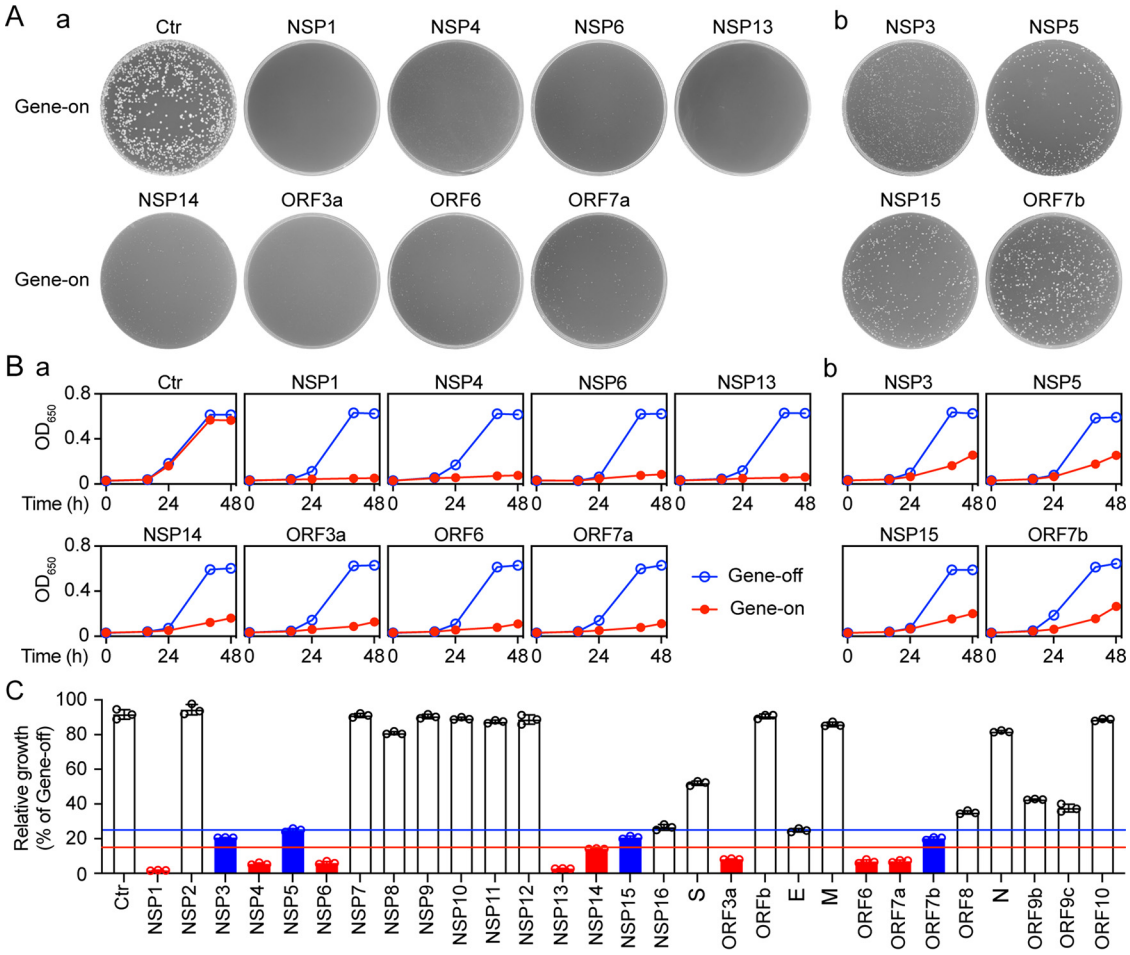

FIG 1 Effect of SARS-CoV-2 expression on fission yeast colony formation (A), cellular growth (B), and summary of the relative cellular growth (15%, red; 25% blue) of each of the SARS-CoV-2 protein-expressing cells (C). The name of each SARS-CoV-2 protein is labeled above each agar plate. An empty pYZ1N vector (Ctr) was used as a control. Gene-off, no SARS-CoV-2 protein production; gene-on, the specific SARS-CoV-2 protein production was induced by triggering the *nmt*1 promoter-mediated gene transcription. Fission yeast colony formation was measured by growing SARS-CoV-2 protein-expressing fission yeast cells on the selective EMM agar plates and incubated at 30°C for 3 to 5 days before the pictures were taken. The cell proliferation analysis was carried out by comparing cellular growth between the SARS-CoV-2 protein-producing cells and the SARS-CoV-2 protein-suppressing cells over time. Cell growth was measured by spectrophotometry (OD_{650}). Only the effect of those SARS-CoV-2 proteins that showed complete (NSP1, NSP4, NSP6, NSP13, NSP14, ORF3a, ORF6, and ORF7a) or nearly complete (NSP3, NSP5, and NSP15) inhibition of yeast colony formation is shown in A and thereafter. Complete data on cell proliferation are included in Fig. S2. Each experiment was repeated at least three times, and the standard errors of each time point were calculated.

RESULTS

Identification of SARS-CoV-2 cytopathic proteins that prevent cellular proliferation and colony formation of fission yeast. A total of 29 viral ORFs representing all viral proteins produced by the SARS-CoV-2 genome were expressed using inducible *nmt*1 promoter-mediated transcription in a wild-type fission yeast strain, SP223. Fission yeast cells expressing an empty cloning plasmid, pYZ1N, were used as a cloning vector control (Ctr). The effect of the SARS-CoV-2 protein expression on the ability of fission yeast to form colonies, an indication of cell proliferation, was measured on minimal selective agar plates (12, 13). All cells with viral genes repressed (*gene*-off) formed normal-sized colonies on the agar plates (Fig. 1A; see Fig. S2A in the supplemental material). In contrast, 8 nonstructural viral protein-producing fission yeast cells (NSP1, NSP3, NSP4, NSP5, NSP6, NSP13, NSP14, and NSP15) and 4 accessory proteins (ORF3a, ORF6, ORF7a, and ORF7b) showed either complete inhibition or near-complete inhibition of yeast colony formation on minimal selective agar plates (Fig. 1A). In each case, either no colony or very small colonies were observed under viral gene-inducing conditions,

consistent with cellular growth inhibition. With the Ctr control, normal size colonies were observed on both gene-suppressing (*gene*-off) and gene-inducing (*gene*-on) plates, confirming the specificity of the viral protein effect observed. We named the 12 viral proteins the "cytopathic proteins." The production of the remaining 18 SARS-CoV-2 proteins showed either no effect or a reduced effect on the fission yeast colony formation (Fig. S2A).

To verify the effect of the 12 cytopathic proteins on cell proliferation, we measured the growth kinetics of the SARS-CoV-2-carrying fission yeast cells. Fission yeast cells were grown under the *gene*-off and *gene*-on conditions in the liquid minimal and selective Edinburgh minimal medium (EMM). Cellular growth was measured by the change in cell concentration over 48 h after gene induction (agi) using optical density at 650 nm (OD_{650})-based measurements. In the Vec-only control cultures, two indistinguishable growth curves with typical logarithmic kinetics were observed in the *gene*-off and *gene*-on pYZ1N-carrying yeast cells. In contrast, expression of NSP1, NSP4, NSP6, NSP13, ORF3a, ORF6, or ORF7a completely blocked cellular growth, whereas expression of NSP3, NSP5, NSP14, NSP15, or ORF7b significantly suppressed cellular growth (Fig. 1B). During the first 24 h agi, both the SARS-CoV-2 *gene*-off and *gene*-on cells grew at about the same rate, consistent with 16 h being required to fully produce a protein after the induction of genes under the control of the *nmt*1 promoter (14). However, thereafter, the growth of cells expressing the 12 viral proteins stopped or slowed compared with that of cells without viral gene expression. The relative cellular growth of each of the SARS-CoV-2 protein-expressing cells are summarized in Fig. 1C. Consistent with the data on colony formation, the production of the remaining 18 SARS-CoV-2 proteins showed either no effect or a reduced effect on fission yeast cellular growth (Fig. S2B).

SARS-CoV-2 cytopathic proteins induce fission yeast cell morphologic changes and hypertrophy. Changes in cell morphology, such as hypertrophy, are linked to SARS-CoV-2-induced cytopathic effects in human airway epithelial cells and myocytes (15). To determine whether the SARS-CoV-2 cytopathic proteins affect cell morphogenesis, we compared microscopic cell morphologies between fission yeast cells with or without viral protein production. Control cells containing the Vec-carrying plasmid appeared normal under both gene-suppressing and gene-inducing conditions. Cells were typically rod shaped with diameters of 3 to 4 μM and lengths of 7 to 14 μM. They were shiny on the edges, which is a sign of healthy cells (Fig. 2A) (10). Normal cell morphologies also were observed in cells that carried the 12 cytopathic protein-encoding plasmids under the gene-suppressing conditions. In contrast, the expression of the 12 SARS-CoV-2 cytopathic proteins under the gene-inducing conditions resulted in various degrees of hypertrophic morphologies (Fig. 2A, bottom rows of each panel). The common features of the abnormal cell morphologies included cell elongation and enlargement. We further analyzed the overall changes in cell morphology caused by the 12 cytopathic proteins. Both the forward-scattered light (FSC) and side-scattered light (SSC) were measured for each cell population of 10,000 cells using flow cytometric analysis (Fig. 2B). The FSC is relative to the cell surface area and thus measures cell size. The SSC is related to cell granularity and thus determines intracellular complexity. The combined analyses of FSC and SSC provide the overall architectures of cell shapes in a heterogeneous cell population. As shown in Fig. 2B, there were significant differences in the cells' overall architectures between the *gene*-off and *gene*-on cultures of cells with cytopathic proteins. In contrast, there were no clear differences between the gene-inducing and gene-repressing Vec-carrying fission yeast cells, suggesting the observed morphological changes were specific to SARS-CoV-2 proteins. The production of all other SARS-CoV-2 proteins did not induce clear morphologic changes (see Fig. S3A in the supplemental material) or cellular hypertrophy (Fig. S3B). Together, our observations suggest that the 12 cytopathic proteins cause various degrees of cellular hypertrophy.

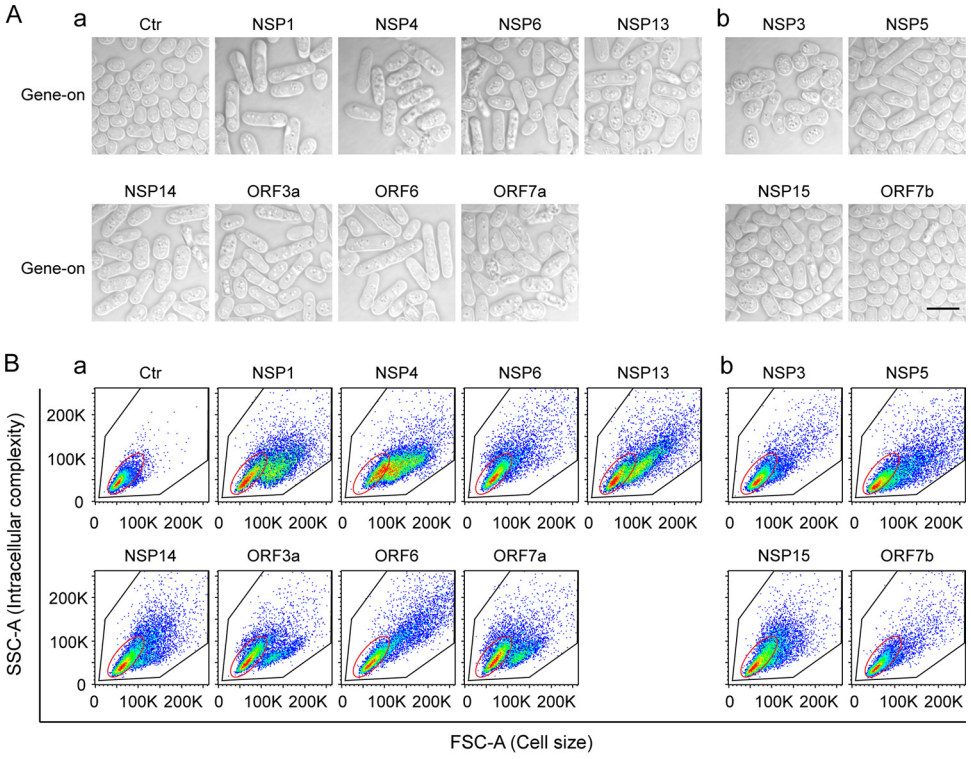

FIG 2 The effect of SARS-CoV-2 protein on fission yeast cellular morphology. Only those SARS-CoV-2 proteins that affected cell proliferation presented in Fig. 1 are shown here. Complete SARS-CoV-2 genome-wide data on fission yeast cellular morphology are included in Fig. S3. (A) Shows the effect of individual SARS-CoV-2 proteins on fission yeast cell morphology. Each image was taken 48 h agi using bright field microscopy. Scale bar = 10 μM. (B) Overall cell morphology as shown by the forward-scattered analysis. A total of 10,000 cells were measured 48 h agi. The forward-scatter light (FSC) measures the distribution of all cell sizes. The side-scatter light (SSC) determines intracellular complexity. Gene-off, no SARS-CoV-2 protein production; gene-on, SARS-CoV-2 protein produced.

Correlation of SARS-COV-2 protein-induced cell death and induction of cellular oxidative stress in fission yeast. Since all 12 cytopathic proteins reduce or prevent cell proliferation (Fig. 1) and cause cellular morphologic changes (Fig. 2), these effects could be lethal. We tested whether the cytopathic proteins cause cell death. The inducible production of each viral protein was carried out as described above. Forty-eight hours agi, cell death was detected by trypan blue, a vital diazo dye that specifically detects dead cells (6, 8). As shown in Fig. 3A, all cytopathic proteins induced cell death in the range of 10% to 60% (Fig. 3C, blue bars). In contrast, most of the other SARS-CoV-2 proteins did not kill cells or the extent of cell killings is not as strong as those of the 12 cytopathic proteins (see Fig. S4A in the supplemental material).

We explored the mechanism of cell death caused by the cytopathic proteins. Because a cellular oxidative stress response can trigger cell death and is known to play an important role in COVID-19 (16–18), we tested for intracellular oxidative stress by measuring the production of reactive oxygen species (ROS). A ROS-specific dye, dihydroethidium (DHE), that produces red fluorescence in the presence of ROS, was used to measure the presence of ROS 48 h agi (Fig. 3B). Except NSP14, other cytopathic proteins triggered the induction of ROS as quantified and shown by the red bars (Fig. 3C). These observations suggest that cell death induced by the cytopathic proteins, with the exception of NSP14, was at attributable least partially to the induction of intracellular oxidative stress. Note that 2 NSPs (NSP2 and NSP16) and 3 structural proteins (E, M, and S) also induced ROS production (Fig. S4B). However, the levels of the cell killings by these proteins were below the cutoff as shown by the 12 cytopathic proteins (Fig. 1C). Thus, these proteins are excluded from discussion.

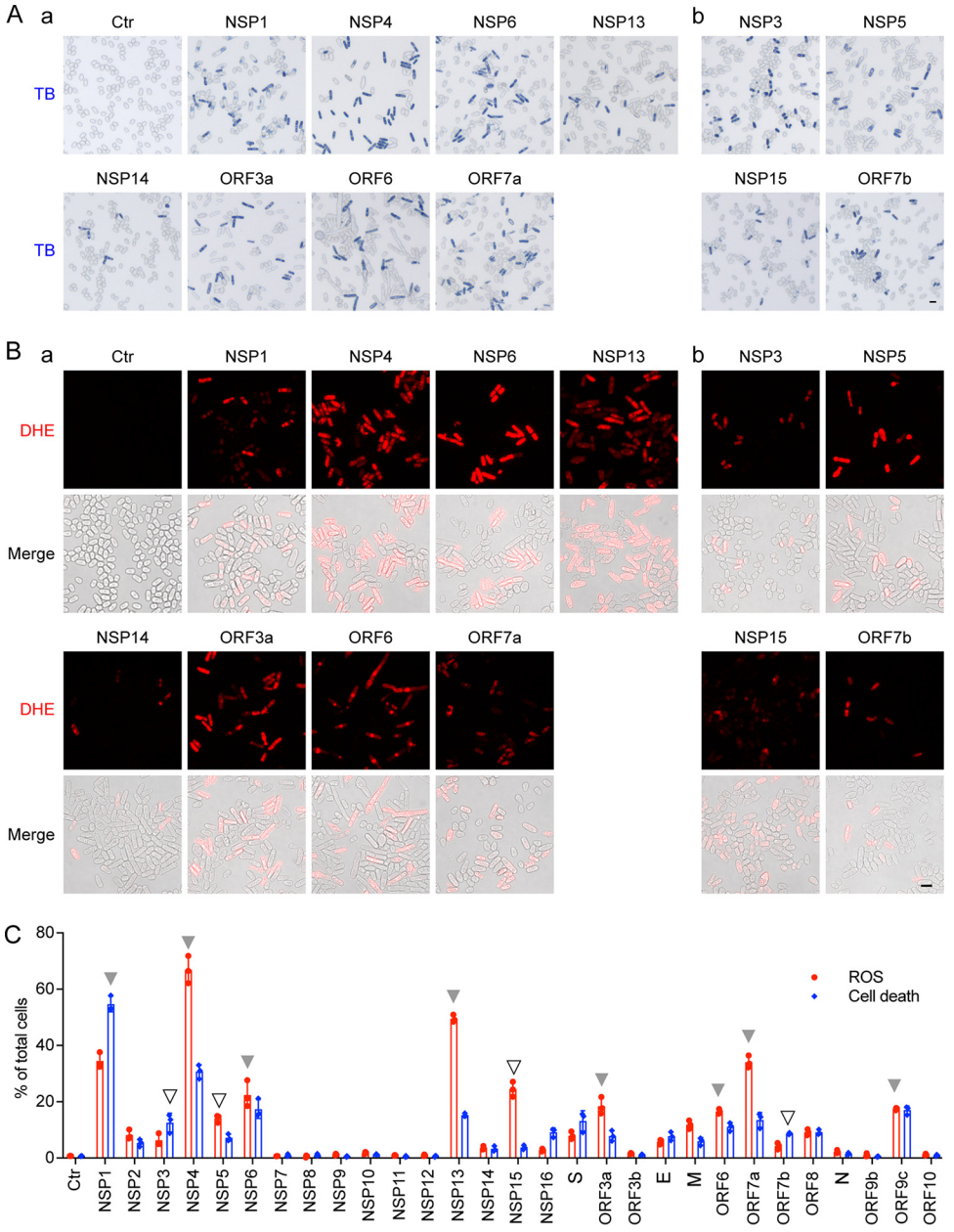

FIG 3 Correlation of SARS-CoV-2 protein-mediated cell death with the induction of oxidative stress in fission yeast. (A) SARS-CoV-2 protein-induced cell death was measured 48 h agi by trypan blue staining. (B) SARS-CoV-2 protein induces oxidative stress, as indicated by the DHE staining showing the production of ROS. Images were taken 48 h agi. Scale bar = 10 μM. BF, bright field; ROS, reactive oxidative species. DHE, an oxidative stress-specific dye (8, 67). (C) Quantitative correlation of SARS-CoV-2 protein-induced cell death (blue bars) and the production of ROS (red bars). Data represent mean ± SE from three independent experiments. Complete SARS-CoV-2 genome-wide data on fission yeast cell death and ROS production are included in Fig. S4.

ORF3a-induced apoptosis and necrosis are associated with the activation of mammalian cellular oxidative stress and immune proinflammatory responses. Of the identified cytopathic proteins, ORF3a was chosen for further study because it plays an important role in viral pathogenesis and its activities are linked to lung tissue damage and a cytokine storm in COVID-19 (19, 20). Since we found that ORF3a-induced cell death was associated with the induction of cellular oxidative stress in fission yeast (Fig. 3), we tested whether a similar ORF3a effect is produced in mammalian cells, including human pulmonary epithelial A549 and Calu-3, as well as kidney epithelial 293T cell lines. After transfection of the *ORF3a*-carrying lentiviral pLVX451 EF1alpha-

IRES-Puro plasmid vector into A549 and 293T cells, cell growth over time was measured. Cell viability and cell death were evaluated by the 3-(4,5-dimethyl-2-thiazolyl)-2,5-diphenyl-2H-tetrazolium bromide (MTT) method and trypan blue exclusion. As shown in Fig. 4A and B, the expression of *ORF3a* in either the A549 or the 293T cells significantly reduced cell growth, decreased cell viability, and increased cell death in comparison with the mock and the vector controls. Possible effects of ORF3a-induced cell death via apoptosis or necrosis were evaluated by a RealTime Glo annexin V apoptosis and necrosis assay. As shown in Fig. 4C, a to b, ORF3a-induced cell death involved both apoptosis and necrosis. ORF3a-induced apoptosis was mediated at least in part through the cleavage of caspase-3 (Fig. 4C, a to c). In addition, the expression of *ORF3a* triggered a cellular oxidative stress response, as measured by DHE staining (Fig. 4D). Our results suggest that ORF3a-induced apoptosis and necrosis in mammalian cells are associated at least in part with the induction of a cellular oxidative stress response.

To test whether the induction of apoptosis and necrosis by ORF3a is related to a host cellular immune response, we first measured a well-recognized master regulator, nuclear factor kappa B (NF-κB), that mediates cellular proinflammatory responses to viral infection (21). A NF-κB luciferase (luc) reporter plasmid system (Stratagene, La Jolla, CA) was used to measure NF-κB-mediated transcriptional activities. The plasmid contains a firefly *luc* gene that is driven by 5-kb NF-κB binding and activating elements located upstream of the minimal TATA promoter. Upon the activation by proinflammatory cytokines, endogenous NF-κB transcription factors bind to the DNA response elements, inducing transcription of the *luc* reporter gene. Thus, the production of Luc indicates the activation of the NF-κB pathways. As shown in Fig. 4E, expression of ORF3a markedly elevated NF-κB-mediated transcriptional activities over time. Next, we measured the production of the cytokines, tumor necrosis factor alpha (TNF-α), interleukin-6 (IL-6), and their regulator NF-κB by quantitative reverse transcriptase PCR (qRT-PCR). The mRNA levels of each gene target were measured over time (Fig. 4F). The gene expression of both TNF-α and IL-6 increased moderately in Calu-3 and 293T cells at 72 h posttransfection (hpt). The level of NF-κB also increased slightly over time. These data suggest that ORF3a-induced apoptosis and necrosis could also contribute to the activation of a cellular proinflammatory response.

ORF3a-induced apoptosis and necrosis are affected by natural and artificial gene mutations. To further elucidate the molecular mechanism underlying ORF3a-induced apoptosis and necrosis (Fig. 5), we tested the effect of ORF3a mutation on the induction of apoptosis and necrosis. A natural mutant variant (Q57H) that is associated with the ongoing Beta variant and deletion of a highly conserved glycine residue (ΔG188) were tested. The ΔG188 mutant was chosen because the amino acid (aa) 188 is highly conserved among sarbecoviruses. G188 may be structurally important as it is one of the two glycine resides that separate two antiparallel β4 and β5 sheets, and both residues are in the proximity of two homodimers of ORF3a and the free C-terminal end of the protein (22). The same methods as described above (Fig. 4) were used to measure cell growth, cell viability, apoptosis, and necrosis with the ORF3a mutants. Compared with wild-type ORF3a, the ΔG188 mutant showed significant differences in its effects, including markedly reduced cellular growth and viability and increased cell death over time (Fig. 5A, a to c, red bars). In contrast, the Q57H mutant showed slightly improved cellular growth and viability and reduced cell death (Fig. 5A, a to c, blue bars). Compared with wild-type ORF3a, the ΔG188 mutant markedly increased apoptosis and necrosis, whereas the Q57H mutant showed slightly reduced apoptosis and necrosis. Consistent with the idea that ORF3a-induced cell death is mediated through the induction of cellular oxidative stress, a positive correlation also was seen between the wild-type and mutant ORF3a in the production of ROS (Fig. 5C, a to b). Based on these observations, ORF3a-induced apoptosis and necrosis are likely mediated through the induction of cellular oxidative stress, and the overall structure of the ORF3a protein appears to be important for the induction of cell death.

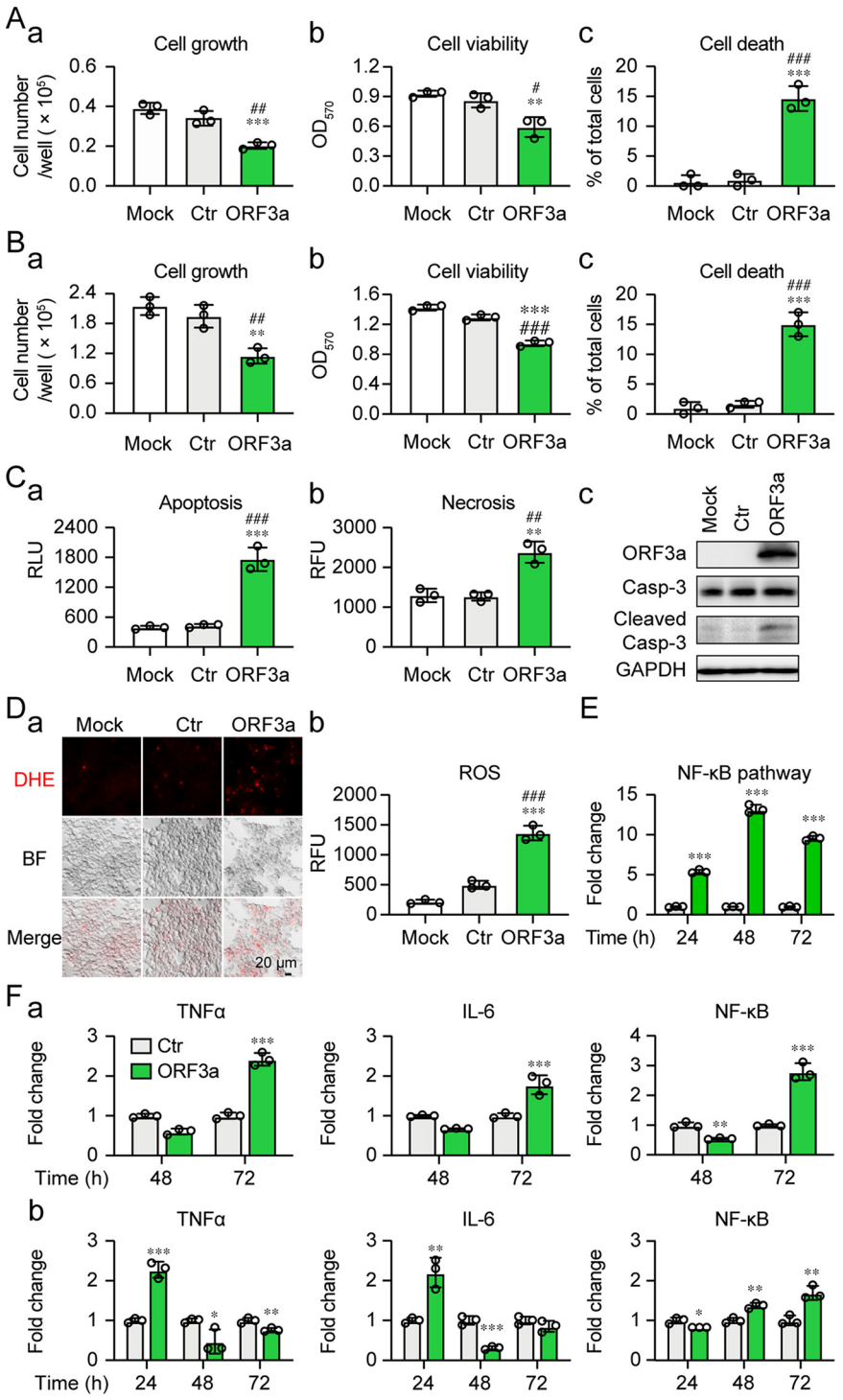

FIG 4 SARS-CoV-2 ORF3a-induced apoptosis and necrosis are correlated with the induction of cellular oxidative stress and innate immune proinflammatory responses in mammalian cells. Expression of SARS-CoV-2 *ORF3a* induces cellular growth reduction and cell death 72 hpt in human lung epithelial A549 cells (A) and human kidney epithelial 293T cells (B). (C) ORF3a induces apoptosis and necrosis 48 hpt measured by Annexin V (a), necrosis (b), and caspase-3 cleavage (c). (D) ORF3a triggers the induction of oxidative stress 48 hpt measured by the DHE straining. The *ORF3a* was cloned in a lentiviral constitutive expression vector (4). Scale bar = 20 μM. (E) ORF3a elevates NF-κB-mediated transcriptional activities. (F) ORF3a triggers elevated production of TNF-α, IL-6, and NF-κB in Calu-3 (a) and 293T (b) cells. Data are presented as mean ± SE from three independent experiments. Statistical differences between ORF3a and mock (indicated with #) or empty vector control (indicated with *) were evaluated. * or #, $P < 0.05$; ** or ##, $P < 0.01$; *** or ###, $P < 0.001$ (pair-wise *t* test).

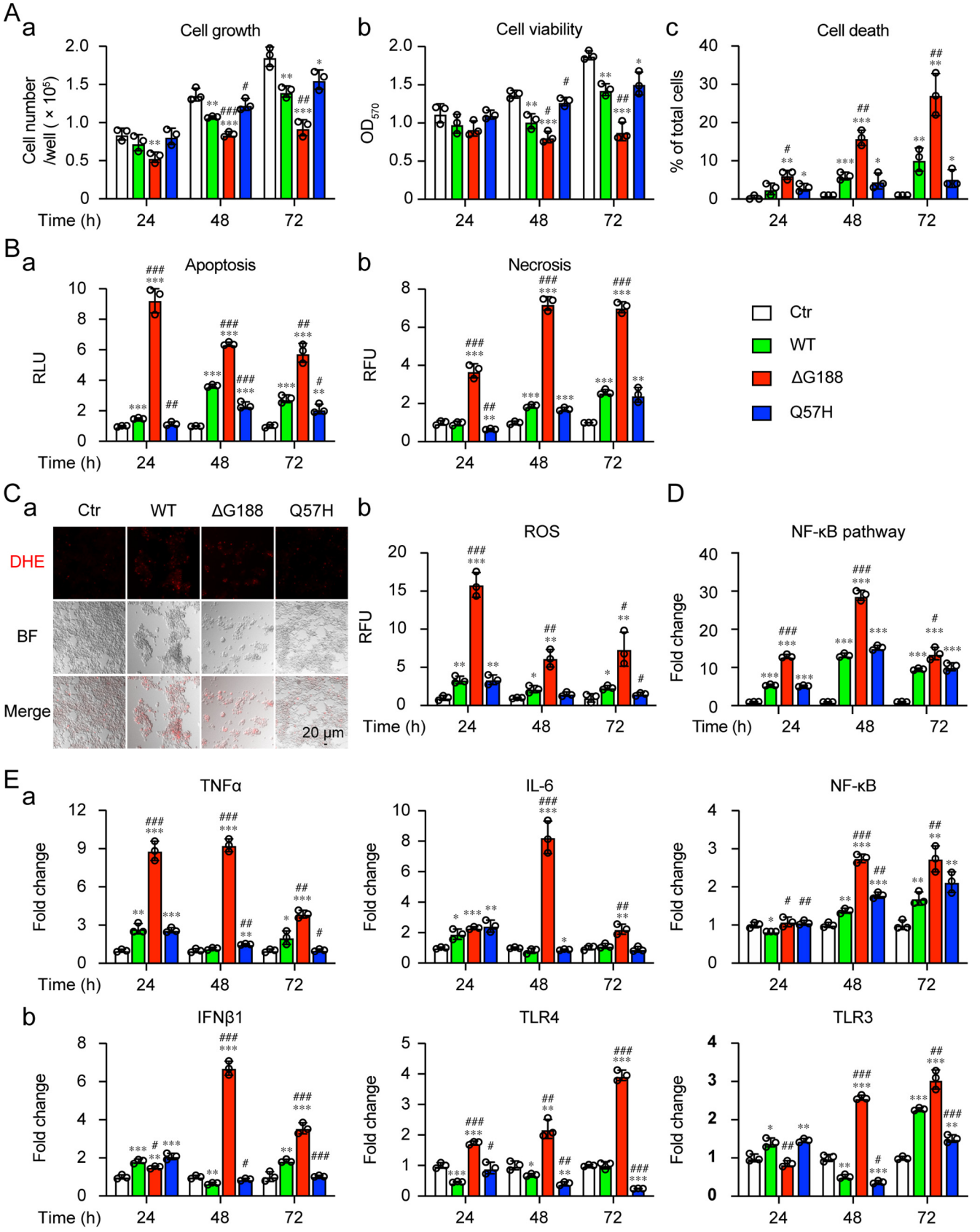

FIG 5 ORF3a-induced apoptosis by natural and artificial mutant variants correlates with cellular oxidative stress and innate immune proinflammatory responses. 293T cells were transfected with plasmids harboring ORF3a wild type (WT), ΔG188, or Q57H mutant variant. Effects of ORF3a mutant variants

(Continued on next page)

ORF3a-induced apoptosis and necrosis are correlated with the level of cellular proinflammatory response. Since ORF3a-induced cell death is associated with the activation of host cell proinflammatory response (Fig. 4E and F), we tested whether the level of ORF3a-induced cell death is correlated with the NF-κB-mediated transcriptional activities or the level of the cellular proinflammatory response. Both Q57H and ΔG188 mutants were tested in comparison with the wild-type ORF3a. While the Q57H mutant showed a similar immune expression profile as the wild-type ORF3a (Fig. 5D; Fig. 5E-a, blue bars), sharp increases in NF-κB-mediated activities and transcription of TNF-α, IL-6, and NF-κB were observed with the ΔG188 mutant (Fig. 5D; Fig. 5E-a, red bars), suggesting a strong correlation between the level of apoptosis and necrosis induced by the ΔG188 mutant and NF-κB-mediated transcription of TNF-α or IL-6. To further test whether other cytokines or pattern recognition receptors that recognize RNA virus also respond to the expression of ORF3a, we measured mRNA levels of type I interferon beta-1 (IFN-β1), Toll-like receptors 4 (TLR4), and Toll-Like receptors 3 (TLR3). Similar or slightly reduced activation of IFN-β1, TLR4, and TLR3 was observed in the Q57H mutant compared with the wild-type ORF3a (Fig. 5E-b), whereas sharp increases of IFN-β1, TLR4, and TLR3 were observed with the ΔG188 mutant (Fig. 5E-b). Interestingly, there were temporal differences in the activation of the various cytokines and regulators. The increase in TNF-α began as early as at 24 hpt and was significantly reduced at 72 hpt (Fig. 5E-a). In contrast, no significant increase of signals of NF-κB, TLR4, or TLR3 was seen at 24 hpt, but mRNA abundance gradually increased from 48 to 72 hpt, suggesting they might be late events. The two type I interferons IFN-β1 and IL-6 showed a significant spike at 48 hpt. These observations suggest that there is an active interaction between the expression of ORF3a and the host cellular innate immune responses.

DISCUSSION

Although current mRNA-based vaccines are generally effective at preventing SARS-CoV-2 infection, the effectiveness of those vaccines wane over time (23). In addition, the emergence of new viral variants could further undermine the effectiveness of those vaccines. Antiviral drugs are an alternative, potentially effective means to treat SARS-CoV-2 infection and curtail COVID-19 but currently such drugs are limited. Two antiviral drugs were granted recently by U.S. FDA for emergency use, which include a nirmatrelvir and ritonavir drug combination (Paxlovid) by Pfizer and molnupiravir (Lagevrio) by Merck. Molnupiravir is a nucleoside analogue that resembles cytidine in RNA. It inhibits viral reproduction by introducing nucleoside substitution β-D-N4-hydroxycytidine 5′-triphosphate into viral RNA during viral replication that is mediated by RNA-directed RNA polymerase (24). Nirmatrelvir is a competitive 3C-like protease ($3CL^{pro}$) inhibitor (25). Ritonavir is a CYP3A enzyme inhibitor that is used to maintain the high plasma concentration of nirmatrelvir. However, the discovery of new antiviral agents is limited by our current knowledge on the viral pathogenicity of the virus and of which viral protein(s) should be targeted. Thus, there is a continued need to identify viral proteins that cause, e.g., harmful cytopathic effects, tissue damage, and cytokine storm, in order to advance the rational design of anti-COVID-19 drug therapies.

The goal of this study was to identify SARS-CoV-2 viral targets that can be used in high-throughput drug screening and antiviral drug discovery. Our criteria for appropriate targets were that the viral protein must contribute to viral pathogenesis and cause a measurable cytopathic effect that can be used in large-scale drug screening. Twelve viral proteins were identified that included 8 nonstructural proteins (NSP1, NSP3, NSP4,

FIG 5 Legend (Continued)
on cytopathic effects (A), as measured by cellular growth (a), cell viability (b), and cell death (c), at the indicated times. (B) Effects of ORF3a mutant variants on apoptosis (a) and necrosis (b). (C) Induction of oxidative stress. The images were taken at 72 hpt. Scale bar = 20 μM. (D) ORF3a elevates NF-κB-mediated transcriptional activities. (E) Activation of cellular innate immune proinflammatory responses, as measured by qRT-PCR. Data are presented as mean $\pm$ SE from three independent experiments. Statistical differences between control and ORF3a WT or mutants (indicated with #) or between WT and mutants (indicated with *) were evaluated. * or #, $P < 0.05$; ** or ##, $P < 0.01$; *** or ###, $P < 0.001$ (one-way ANOVA).

NSP5, NSP6, NSP13, NSP14, and NSP15) and 4 accessory proteins (ORF3a, ORF6, ORF7a, and ORF7b). Overall, they all inhibited cellular growth (Fig. 1), caused cellular hypertrophy (Fig. 2), and induced cell death (Fig. 3).

Two major types of viral proteins were identified, namely, viral enzymes and viral proteins that participate in viral replication or transcription (26). Among the viral enzymes, NSP5 carries the major 3C-like protease, NSP3 produces a minor papain-like protease ($PL2^{pro}$), NSP13 carries a viral helicase that unwinds duplex RNA or DNA with a 5′→3′ polarity, and NSP14 is a dual-function enzyme with N-terminal exoribonuclease (ExoN) and C-terminal N7-methyltransferase (N7-MTase) activities. All of these viral enzymes are highly conserved among coronaviruses and are essential for viral replication (26). Therefore, they might be ideal targets for antiviral drug discovery. Notably, viral proteases are proven antiviral targets against HIV-1 (27) and hepatitis C virus (HCV) infection (28). Some of the FDA-approved HIV-1 and HCV protease inhibitor drugs inhibit $3CL^{pro}$ or $PL2^{pro}$ (29, 30). Although no clinical benefit has yet been shown from using those repurposed drugs, they nevertheless indicate the potential of using protease inhibitor drugs for treating COVID-19. The successful development of the first protease inhibitor antiviral drug Paxlovid (PF-07321332) against SARS-CoV-2 by Pfizer (31) attests this possibility. The fission yeast $3CL^{pro}$ or $PL2^{pro}$ cell-based assays described here could conceivably be used for high-throughput screening and testing of future SARS-CoV-2 protease inhibitors. This use is certainly feasible because our early study shows that all FDA-approved HIV-1 protease inhibitor drugs suppress HIV-1 protease in the fission yeast cell-based system (12). NSP13 also shows dNTPase and RNA 5′-triphosphatase activities besides its helicase activity. NSP13 is the most conserved coronaviral protein, and it is essential for viral RNA transcription and replication. Therefore, it is another promising viral target for antiviral drug development (32).

Three of the identified viral candidates (NSP3, NSP4, and NSP6) form a core protein complex that is responsible for the formation of virus-induced double-membrane vesicles (DMVs). DMVs are part of the viral replication-transcription complex (RTC) in SARS-CoV-2-infected cells that drives replication and transcription for virus reproduction (33, 34). The RTC formed by NSP3/4/6 in SARS-CoVs links the cytoplasmic membrane with the endoplasmic reticulum lumen to induce membrane curvature and form unique DMVs (35). In addition, NSP3/4/6 interacts with E, M, and N proteins to facilitate viral assembly (36). Thus, interruption of the NSP3/4/6 protein complex and DMV formation could potentially be a critical viral target to inhibit viral replication and transcription.

ORF3a was chosen for mechanistic studies because it fulfills the predefined criteria as a potential therapeutic target. ORF3a is a multifunctional protein that has 275 aa (~31 kDa) and presents as a homodimer or tetramer (22). It has 3 transmembrane regions that span halfway across the membrane and cytosol that are linked to multifunctionalities, including virulence, infectivity, ion channel formation, and virus release (37–40). ORF3a plays an important role in SARS-CoV-2-mediated viral pathogenesis, including induction of the inflammasome in damaged lung tissue and initiation of cytokine storm (20, 41). High titers of the anti-ORF3a antibody were found in SARS-CoV-2-infected patients, suggesting its clinic significance (42). Deletion or transcription knockdown of *ORF3a* from either the SARS-CoV or the SARS-CoV-2 genome results in a major reduction of virus growth (43, 44). SARS-CoV-2 ORF3a is essential for viral replication in the absence of the E protein (45, 46).

Consistent with our findings from the fission yeast studies, ORF3a prevented cell proliferation and induced apoptosis and necrosis in mammalian cells (Fig. 4A to C), in part through the induction of cellular oxidative stress (Fig. 4A to D). ORF3a-induced apoptosis has been reported previously (47). However, oxidative stress-induced cell death had not been reported in SARS-CoV-2 infection, and the viral protein(s) responsible for inducing cellular oxidative stress had not been identified. Here, we report for the first time that ORF3a induces ROS production leading to cellular oxidative stress, and this cellular stress response appears to be a common feature of all the viral proteins except NSP14 that link to cell death in fission yeast cells (Fig. 3C, shown by arrows). Whether

the activation of cellular oxidative stress also contributes to the death of human cells caused by other viral proteins besides ORF3a remains to be elucidated. Oxidative stress is a common cellular response to viral infection (48). Sustained viral infection leads to the accumulation of the ROS in cells or tissues that may result in tissue damage and cell death (49, 50). Increasing evidence suggests that excessive ROS production is a major cause of local or systemic tissue damage and contributes to the severity of COVID-19 (17, 18). Therefore, focusing on these viral targets could potentially help ease the COVID-19 burden. It is unclear at present why NSP14-induced cell death did not trigger a cellular oxidative stress response. One possible explanation is that it functions as an enzyme that is part of normal cellular activity.

ORF3a-induced apoptosis and necrosis might also be attributed in part to the activation of a cellular proinflammatory response, as three of the common proinflammatory cytokines, namely, TNF-α, IL-6, and IFN-β1, were all elevated (Fig. 4E and F; Fig. 5D). Clinical studies suggest that high serum IL-6 and TNF-α levels are strong, independent predictors of patient survival (51, 52) and that hyperinflammatory responses in patients with COVID-19 are a major cause of disease severity and death (51, 52). ORF3a-induced apoptosis and necrosis might be one of the viral factors that contributes to the elevation of IL-6 and TNF-α observed in these patients. Our data show that the elevated production of IL-6 and TNF-α could be mediated through NF-κB, a well-recognized master regulator that mediates cellular proinflammatory responses to viral infection (21). In addition, TLR3 and TLR4 might also be involved in these elevations, as they are also activated (Fig. 5E). Both TLR3 and TLR4 recognize RNA viruses and trigger the antiviral production of type I IFNs and proinflammatory cytokines. TLR4 is a cell membrane receptor (53) and TLR3 resides on the endosomal membrane in epithelial cells (54). TLR3 induces proinflammatory cytokine production through TRIF (54), whereas TLR4-mediated proinflammatory cytokine production is likely through NF-κB. Both TLR3- and TLR4-mediated proinflammatory responses contribute to the severity of COVID-19 (55–57). TLR4-mediated production of IL-6 and TNF-α is associated with the severity of COVID-19 in patients with cardiometabolic comorbidities (55). Inhibition of TLR3 by famotidine decreases IL-6 (56) and reduces the risk of intubation and death in patients hospitalized with COVID-19 and alleviates symptoms in nonhospitalized patients with COVID-19 (57). Both cellular inflammation and oxidative stress contribute to the severity of the COVID-19 (58). In addition, ORF3a-induced apoptosis and necrosis are highly conserved cellular responses among yeast (this study), *Drosophila* (59), and human cells (47). Therefore, targeting ORF3a-induced apoptosis and necrosis could be a promising antiviral strategy to fight against COVID-19. Fission yeast could potentially be used as a surrogate system for large-scale drug screening and testing of anti-ORF3a inhibitors.

The ΔG188 mutant triggered a much stronger activation of the cellular oxidative stress and innate immune responses than wild-type ORF3a (Fig. 4 and 5). An early protein structural analysis suggests that the G188 residue may be structurally important, as it is one of the two highly conserved glycine resides among sarbecoviruses that separate two antiparallel β4 and β5 sheets, and both residues are in the proximity of two homodimers of ORF3a and the free C-terminal end of the protein (22). The ΔG188 mutant may interrupt dimerization of the protein or the structure of the two antiparallel β4 and β5 sheets at the C-terminal end where it affects ion channel activity or interaction of ORF3a with host cellular proteins (22). The ORF3a activity has been linked to a number of sequence motifs from the signal peptide (aa 1 to 13) of the N terminus to a di-acidic motif (aa 171 to 173) (40, 47). This study is the first demonstration of the functional relevance of the G188 residue at the β4/β5 junction of the C terminus of ORF3a in the activation of cellular stress, innate immune response, and induction of apoptosis and necrosis. Additional mutagenesis studies are needed to confirm our findings. One possible explanation for the stronger effect of the ΔG188 mutant than that of the wild type is that the wild-type ORF3a effect might be restricted by a host restriction cellular protein(s) through a direct protein-protein interaction, as shown in other viral infections (60, 61). If this is indeed the case,

interruption of the ORF3a protein with the host restriction factor(s) by the ΔG188 mutation could release the ORF3a resulting enhanced triggering of host cellular stress and innate immune response and leading to stronger cell death. This scenario is further suggested by the fact that the wild-type ORF3a completely kills fission yeast cells but only partially kills human cells. Note that ORF3a-induced cell killing in fission yeast is not an artifact caused by protein overproduction, as viral proteins with similar molecular weights, such as NSP8 and seventeen other viral proteins, did not cause cell killing nor do they induce the ROS under the same experimental conditions. It would be of interest to identify the binding partner(s) of the ORF3a in human cells.

ORF3a mutations are associated with disease progression (39, 40) and high mortality in patients with COVID-19 (62). The Q57H mutation (40, 62) was found recently in the emerging Beta variant (63), and the Q57H variant was suspected of contributing to a surge of SARS-CoV-2 infection in Hong Kong (64). Our data show that the Q57H mutant activities are comparable to those of the wild-type ORF3a regarding the induction of cellular oxidative stress, innate immune responses, and apoptosis and necrosis (Fig. 4 and 5). However, our data cannot rule out the possibility that the Q57H mutant may have other effects on viral pathogenesis. For example, the Q57H mutant was predicted to bind the S protein, whereas the wild type does not (65). It would be of interest to test whether the Q57H mutant contributes to viral entry. A number of new ORF3a mutations were found to associate with the emergence of the new viral variants. It would be necessary to test the effect of those natural ORF3a variants on their interactions with host cellular stress and innate immune responses to better understand the role of ORF3a in COVID-19.

In summary, through genome-wide characterization, 12 viral proteins were identified to exert cytopathic effects. Since these viral proteins are essential for viral survival and contribute to viral pathogenesis, they could serve as therapeutic targets for future antiviral drug discovery. In accordance with this finding, we demonstrated here that ORF3a induces apoptosis and necrosis through the activation of cellular oxidative stress and host innate immune proinflammatory responses. Since these ORF3a activities are linked to viral pathogenesis, disease progression, and severity of COVID-19, it would be desirable to develop a fission yeast cell-based high-throughput system to identify anti-ORF3a drugs to battle COVID-19.

MATERIALS AND METHODS

Cell and growth media. A wild-type fission yeast SP223 strain (*h-*, *ade6-216*, *leu1-32*, and *ura4-294*) was used to test the cytopathic effect of SARS-CoV-2 viral proteins in this study (8, 14). Standard yeast extract-sucrose (YES) complete, minimal EMM, or Pombe Glutamate medium (PMG) selective media supplemented with adenine, uracil, leucine, or thiamine (20 μM) was used to grow fission yeast cells or to select for plasmid-carrying cells. Luria-Bertani (LB) medium supplemented with ampicillin (100 μg/mL) was used for growing New England BioLabs (NEB) stable *Escherichia coli* (NEB catalog [cat] no. C3040H) or DH5α cells and for DNA transformation.

Human pulmonary epithelial cell lines A549 (ATCC CCL-185) and Calu-3 (ATCC HTB-55) and a human embryonic kidney epithelial 293T cell line was used in this study. A549 and 293T cell lines were maintained in the high-glucose Dulbecco's modified Eagle's medium (DMEM) (Corning cat 10-017-CV) with 10% fetal bovine serum (FBS; Gibco cat 100-438-026) and 100 U/mL penicillin-streptomycin (Gibco cat 15140122). Calu-3 cells were maintained in Eagle's minimum essential medium (EMEM) (Quality Biological cat 112-018-101) with 10% FBS and 100 U/mL penicillin-streptomycin. All cell lines were grown in an incubator at 37°C with 5% CO_2.

SARS-CoV-2 reference strain and plasmids. A U.S. SARS-CoV-2 reference strain, USA-WA1/2020 (GenBank accession no. MN985325), was used for the genome-wide functional analysis of the SARS-CoV-2 viral proteins. A fission yeast gene cloning system, which includes a pYZ1N gene expression plasmid, has been described previously (6, 13). pYZ1N carries an inducible no message in the thiamine (*nmt1*) promoter. Through the regulation of this promoter, viral gene expression can be either induced or repressed in the absence (*gene*-off) or presence (*gene*-on) of 20 μM thiamine, respectively (13). The fission yeast strain that carries the pYZ1N-SARS-CoV-2 ORF was maintained in the minimal EMM with the selection of the *Leu2* gene carried on the plasmid. For the mammalian ORF3a study, a lentiviral constitutive expression vector pLVX-EF1alpha-IRES-Puro (TaKaRa) that carries the ORF insert (provided by Nevan J. Krogan of University of California San Francisco [UCSF]) was used (4). The ORF3a mutant variants (Q57H and ΔG188) were generated by overlapping PCR with mutant-specific primers (see Table S1 in the supplemental material) and cloned onto the same pLVX-EF1alpha-IRES-Puro plasmid via the Gibson assembly method. All final constructs were verified by Sanger sequencing.

Molecular cloning of SARS-CoV-2 ORFs in fission yeast. A total of 29 SARS-CoV-2 viral ORFs were cloned into a fission yeast pYZ1N gene expression vector system using methods as described previously (6, 8) (see Fig. S1A in the supplemental material). Among them, 27 of the viral ORFs were described previously (4). NSP3 or NSP16 was obtained from Zhe Han of University of Maryland, Baltimore, or Fritz Roth of University of Toronto (Addgene plasmid no. 141269), respectively. Briefly, each SARS-CoV-2 protein-encoding nucleotide was PCR amplified with a pair of primers that contained specific restriction enzyme sites (Table S1; Fig. S1B) for molecular cloning and cloned into the pYZ1N expression vector for the functional analysis. The SARS-CoV-2 viral gene inserts were verified by restriction digestions and Sanger sequencing.

Fission yeast plasmid transformation and inducible SARS-CoV-2 gene expression. The SARS-CoV-2 gene-carrying pYZ1N plasmids were transformed into a wild-type fission yeast SP223 strain by electroporation (8, 66). The plasmid transformants were selected for the presence of the *Leu*2 gene on a minimal selective PMG medium. Successful transformation of the respective SARS-CoV-2-containing plasmids was verified by colony PCR with gene-specific primers (Table S1). Successful expression of the respective SARS-CoV-2 *ORF* mRNA transcripts was measured by RT-PCR using gene-specific primers (Table S1) and a SuperScript III one-step RT-PCR system (Invitrogen; cat no. 12574-030). To measure SARS-CoV-2 gene-specific activities, the PCR-confirmed yeast colony, which carries the desired and specific SARS-CoV-2 gene-containing plasmid, was grown to log phase in liquid EMM supplemented with 20 μM of thiamine. Cells were then washed three times with distilled water to remove thiamine. Finally, 2×10^4 cells/mL, which was quantified using a TC20 automated cell counter (Bio-Rad), was reinoculated into fresh liquid EMM without thiamine to induce gene expression (*gene*-on) or with thiamine to suppress gene expression (*gene*-off). The cell cultures were grown at 30°C with constant shaking before the observation.

Measurement of fission yeast cell-specific activities. The effects of a SARS-CoV-2 protein on fission yeast cellular growth were measured by several methods, which include a yeast colony-forming assay to measure cell proliferation, a cell viability assay (8, 12), and the cellular growth kinetics to quantify cellular growth (8, 14). Briefly, the fission yeast cultures were prepared as described above. A total of 50 μL of liquid cultures with approximately 1×10^3 cells was spread onto the selective EMM agar plates with (*gene*-off) and without (*gene*-on) thiamine. The agar plates were incubated at 30°C for 4 to 6 days before the observation for the presence or absence of fission yeast colony formations and the sizes of the forming colonies. The absence of colonies on the agar plates indicates complete inhibition of cellular proliferation. Fewer colonies with smaller colony sizes than the normal control typically suggest reduced cellular proliferation.

To quantify the level of growth inhibition caused by the expression of a SARS-CoV-2 protein in fission yeast, 100 μL of *gene*-on or *gene*-off liquid cultures (2×10^4 cells/mL) was grown in the 96-well microtiter plate in the selective EMM over time at 30°C in an incubator with moisture. Cellular growth kinetics was measured at OD_{650} over 48 hours by using a Synergy H1M monochromator-based multimode microplate reader (BioTek).

The methods used to test the effect of each viral protein production on fission yeast cell morphology have been described previously (8, 14). Briefly, fission yeast cell morphology was observed using a BZX fluorescence microscope (Keyence) under the bright field 48 h agi. The overall cell morphology was evaluated by flow cytometry using forward-scattered analysis (8, 14). Ten thousand cells were analyzed on a FACSCanto II flow cytometer (Becton, Dickinson). The forward-scattered light (FSC) and side-scattered light (SSC) were measured for each cell population. FSC is proportional to the cell surface area and thus measures cell size. SSC determines intracellular complexity because it is proportional to cell granularity.

SARS-CoV-2 protein-induced cell death was detected by trypan blue staining (8). Trypan blue is a dye that specifically detects dead cells. The activation of fission yeast cellular oxidative stress by SARS-CoV-2 proteins was monitored by the production of ROS, which can be detected by a ROS-specific dye, DHE (Sigma). DHE generates red fluorescence in the presence of ROS (8, 67). DHE was added in a final concentration of 5 μg/mL. Cellular oxidative stress was measured 48 h agi.

Measurement of mammalian cell-specific activities. A total of 2×10^4 293T or 1×10^4 A549 and Calu-3 cells/well were seeded onto a 96-well plate and cultured at 37°C and 5% CO_2 overnight. The plasmid was transfected into cells using the Lipofectamine 3000 reagent (ThermoFisher) following the manufacturer's protocol. Cellular growth or cell death at the indicated time was quantified by cell number counting and trypan blue staining. Briefly, cells were trypsinized, and 10 μL of the cell suspension was mixed with an equal volume of trypan blue. Within 5 minutes of mixing, the total cells and dead cells were counted using a TC20 automated cell counter. Cell viability was determined by the MTT assay as described (68). At the time of the measurement, 10 μL of 5 mg/mL MTT was added to each well of the 96-well plate and incubated at 37°C for 2 to 5 h. After the medium was removed, 100 μL of dimethyl sulfoxide (DMSO) was added to each well and mixed by pipetting. The plates were agitated gently for 15 minutes, and the absorbance was measured at 570 nm using the H1M microplate reader.

Cell apoptosis and necrosis were measured by a RealTime-Glo annexin V apoptosis and necrosis assay (Promega) (69). At 24 h after plasmid transfection, the apoptosis and necrosis detection reagents were added into each well of a 96-well plate. Following incubation at 37°C and 5% CO_2 at the indicated time, luminescence (relative light units [RLU]) and fluorescence (relative fluorescence units [RFU]; 485 nm excitation/520 to 530 nm emission) were used to measure apoptosis and necrosis, respectively, with the H1M microplate reader.

The activation of cellular oxidative stress in mammalian cells was monitored using a ROS detection cell-based assay kit (Cayman Chemical; cat no. 601290). The fluorescence of DHE staining was visualized using a BZX fluorescence microscope (Keyence). The intensity was measured using the H1M microplate reader.

The Western blot analysis was carried out as described previously (68). Total proteins were extracted from transfected 293T cells using radioimmunoprecipitation assay (RIPA) lysis buffer (Millipore Sigma) at

48 hpt. Equal amounts of total protein were separated on an SDS-PAGE gel by electrophoresis and transferred to a polyvinylidene difluoride (PVDF) membrane (Bio-Rad). Target proteins were detected using the following antibodies: mouse anti-Strep tag II (Millipore Sigma; cat no. 71590); rabbit anti-Caspase 3 (Cell Signaling; cat no. 9662); rabbit anti-Cleaved-Caspase 3 (Cell Signaling; cat no. 9664), and mouse anti-GAPDH antibody (Cell Signaling; cat no. 2118).

For the NF-κB luciferase assay to measure NF-κB-mediated transcriptional activities, 2×10^4 293T cells/well was cultured in a white 96-well plate overnight. A total of 0.05 μg of the plasmid with the gene of interest was cotransfected with 0.05 μg of pNF-κB-Luc and 0.005 μg of pRL-SV40. The activities of firefly luciferase and *Renilla* luciferase were measured at the indicated time using the dual luciferase reporter assay system (Promega; cat no. E1910) and H1 plate reader (BioTek). The signal of firefly luciferase was normalized with *Renilla* luciferase, and the fold changes compared to empty vector control were calculated.

Reverse transcriptase quantitative PCR (qRT-PCR) was carried out as we described previously (69). Briefly, a total of 1 μg of extracted total RNA was used for the synthesis of first-strand cDNA using a high-capacity RNA-to-cDNA kit (Thermo Fisher Scientific) according to the manufacturer's instructions. Quantitative PCR was performed on a QuantStudio 3 real-time PCR system using gene-specific primers (see Table S2 in the supplemental material) and 2$\times$ SYBR green qPCR master mix (Bimake). The amplification conditions were 40 cycles of 95°C for 10 s and 60°C for 30 s, followed by melting curve analysis. The fold change in mRNA expression was quantified by calculating the threshold cycle ($2^{-\Delta\Delta CT}$) value, with glyceraldehyde-3-phosphate dehydrogenase (GAPDH) mRNA as an endogenous control.

Statistical analysis. A pair-wise *t* test or one-way analysis of variance (ANOVA) was calculated using software Prism 9 (GraphPad, San Diego, CA, USA). Statistical significance was accepted at the 95% confidence level ($P < 0.05$; * or #, $P < 0.05$; ** or ##, $P < 0.01$; *** or ###, $P < 0.001$).

SUPPLEMENTAL MATERIAL

Supplemental material is available online only.

FIG S1, PDF file, 0.5 MB.

FIG S2, PDF file, 0.7 MB.

FIG S3, PDF file, 0.9 MB.

FIG S4, PDF file, 0.5 MB.

TABLE S1, DOCX file, 0.02 MB.

TABLE S2, DOCX file, 0.01 MB.

ACKNOWLEDGMENTS

We thank Nevan J. Krogan of UCSF (4), Zhe Han of University of Maryland, Baltimore (UMB), and Fritz Roth of University of Toronto (Addgene plasmid no. 141269) for providing the SARS-CoV-2 plasmids used in this study.

This study was supported in part by grants from NIH R21 AI129369, NIH R01 GM127212/AI150459, and VA BLR&D I01BX004652 and intramural funding from the University of Maryland Medical Center (R.Y.Z.). J.M.S. is supported by grants from the Department of Veterans Affairs (RR&D I01RX003060 and BLR&D 1I01BX004652), the Department of Defense (SC170199), the National Heart, Lung and Blood Institute (R01HL082517), and the NINDS (R01NS102589 and R01NS105633). V.G. is supported by NIH R01NS107262. Q.T. is supported by NIH/NIAID and G12MD007597. The contents do not represent the views of the U.S. Department of Veterans Affairs or the United States Government.

We declare no competing interests.

Author contributions are as follows: R.Y.Z. and J.Z. designed experiments and wrote the manuscript; J.Z., Q.L., R.S.C.C., and V.G. carried out or assisted with the experiments; and J.M.S., Q.T., and J.Z. participated in the writing and revision of the manuscript.

REFERENCES

1. Cameroni E, Bowen JE, Rosen LE, Saliba C, Zepeda SK, Culap K, Pinto D, VanBlargan LA, De Marco A, di Iulio J, Zatta F, Kaiser H, Noack J, Farhat N, Czudnochowski N, Havenar-Daughton C, Sprouse KR, Dillen JR, Powell AE, Chen A, Maher C, Yin L, Sun D, Soriaga L, Bassi J, Silacci-Fregni C, Gustafsson C, Franko NM, Logue J, Iqbal NT, Mazzitelli I, Geffner J, Grifantini R, Chu H, Gori A, Riva A, Giannini O, Ceschi A, Ferrari P, Cippà PE, Franzetti-Pellanda A, Garzoni C, Halfmann PJ, Kawaoka Y, Hebner C, Purcell LA, Piccoli L, Pizzuto MS, Walls AC, Diamond MS, et al. 2021. Broadly neutralizing antibodies overcome SARS-CoV-2 Omicron antigenic shift. Nature https://doi.org/10.1038/s41586-021-04386-2.
2. Coronaviridae Study Group of the International Committee on Taxonomy of Viruses. 2020. The species severe acute respiratory syndrome-related coronavirus: classifying 2019-nCoV and naming it SARS-CoV-2. Nat Microbiol 5:536–544. https://doi.org/10.1038/s41564-020-0695-z.
3. Sola I, Almazan F, Zuniga S, Enjuanes L. 2015. Continuous and discontinuous RNA synthesis in coronaviruses. Annu Rev Virol 2:265–288. https://doi.org/10.1146/annurev-virology-100114-055218.
4. Gordon DE, Jang GM, Bouhaddou M, Xu J, Obernier K, White KM, O'Meara MJ, Rezelj VV, Guo JZ, Swaney DL, Tummino TA, Hüttenhain R, Kaake RM, Richards AL, Tutuncuoglu B, Foussard H, Batra J, Haas K, Modak M, Kim M,

Haas P, Polacco BJ, Braberg H, Fabius JM, Eckhardt M, Soucheray M, Bennett MJ, Cakir M, McGregor MJ, Li Q, Meyer B, Roesch F, Vallet T, Mac Kain A, Miorin L, Moreno E, Naing ZZC, Zhou Y, Peng S, Shi Y, Zhang Z, Shen W, Kirby IT, Melnyk JE, Chorba JS, Lou K, Dai SA, Barrio-Hernandez I, Memon D, Hernandez-Armenta C, et al. 2020. A SARS-CoV-2 protein interaction map reveals targets for drug repurposing. Nature 583:459–468. https://doi.org/10.1038/s41586-020-2286-9.

5. Zhao RY. 2017. Yeast for virus research. Microb Cell 4:311–330. https://doi.org/10.15698/mic2017.10.592.
6. Li G, Zhao RY. 2018. Molecular cloning and characterization of small viral genome in fission yeast. Methods Mol Biol 1721:47–61. https://doi.org/10.1007/978-1-4939-7546-4_5.
7. Nurse PM, 2002. Cyclin dependent kinases and cell cycle control. Biosci Rep 22:487–499. https://doi.org/10.1023/A:1022017701871.
8. Li G, Poulsen M, Fenyvuesvolgyi C, Yashiroda Y, Yoshida M, Simard JM, Gallo RC, Zhao RY. 2017. Characterization of cytopathic factors through genome-wide analysis of the Zika viral proteins in fission yeast. Proc Natl Acad Sci U S A 114:E376–E385. https://doi.org/10.1073/pnas.1619735114.
9. Jin H, Du Z, Zhang Y, Antal J, Xia Z, Wang Y, Gao Y, Zhao X, Han X, Cheng Y, Shen Q, Zhang K, Elder RE, Benko Z, Fenyvuesvolgyi C, Li G, Rebello D, Li J, Bao S, Zhao RY, Wang D. 2020. A distinct class of plant and animal viral proteins that disrupt mitosis by directly interrupting the mitotic entry switch Wee1-Cdc25-Cdk1. Sci Adv 6:eaba3418. https://doi.org/10.1126/sciadv.aba3418.
10. Zhao Y, Lieberman HB. 1995. Schizosaccharomyces pombe: a model for molecular studies of eukaryotic genes. DNA Cell Biol 14:359–371. https://doi.org/10.1089/dna.1995.14.359.
11. Olsson I, Bjerling P. 2011. Advancing our understanding of functional genome organisation through studies in the fission yeast. Curr Genet 57:1–12. https://doi.org/10.1007/s00294-010-0327-x.
12. Zhang J, Vernon K, Li Q, Benko Z, Amoroso A, Nasr M, Zhao RY. 2021. Single-agent and fixed-dose combination HIV-1 protease inhibitor drugs in fission yeast (Schizosaccharomyces pombe). Pathogens 10:804. https://doi.org/10.3390/pathogens10070804.
13. Zhao Y, Elder RT, Chen M, Cao J. 1998. Fission yeast expression vectors adapted for positive identification of gene insertion and green fluorescent protein fusion. Biotechniques 25:438–440, 442, 444. https://doi.org/10.2144/98253st06.
14. Zhao Y, Cao J, O'Gorman MR, Yu M, Yogev R. 1996. Effect of human immunodeficiency virus type 1 protein R (vpr) gene expression on basic cellular function of fission yeast Schizosaccharomyces pombe. J Virol 70:5821–5826. https://doi.org/10.1128/JVI.70.9.5821-5826.1996.
15. Zhu N, Wang W, Liu Z, Liang C, Wang W, Ye F, Huang B, Zhao L, Wang H, Zhou W, Deng Y, Mao L, Su C, Qiang G, Jiang T, Zhao J, Wu G, Song J, Tan W. 2020. Morphogenesis and cytopathic effect of SARS-CoV-2 infection in human airway epithelial cells. Nat Commun 11:3910. https://doi.org/10.1038/s41467-020-17796-z.
16. Delgado-Roche L, Mesta F. 2020. Oxidative stress as key player in severe acute respiratory syndrome coronavirus (SARS-CoV) infection. Arch Med Res 51:384–387. https://doi.org/10.1016/j.arcmed.2020.04.019.
17. Laforge M, Elbim C, Frère C, Hémadi M, Massaad C, Nuss P, Benoliel J-J, Becker C. 2020. Tissue damage from neutrophil-induced oxidative stress in COVID-19. Nat Rev Immunol 20:515–516. https://doi.org/10.1038/s41577-020-0407-1.
18. Kozlov EM, Ivanova E, Grechko AV, Wu W-K, Starodubova AV, Orekhov AN. 2021. Involvement of oxidative stress and the innate immune system in SARS-CoV-2 infection. Diseases 9:17. https://doi.org/10.3390/diseases9010017.
19. Chen IY, Moriyama M, Chang MF, Ichinohe T. 2019. Severe acute respiratory syndrome coronavirus viroporin 3a activates the NLRP3 inflammasome. Front Microbiol 10:50. https://doi.org/10.3389/fmicb.2019.00050.
20. Siu K-L, Yuen K-S, Castaño-Rodriguez C, Ye Z-W, Yeung M-L, Fung S-Y, Yuan S, Chan C-P, Yuen K-Y, Enjuanes L, Jin D-Y. 2019. Severe acute respiratory syndrome coronavirus ORF3a protein activates the NLRP3 inflammasome by promoting TRAF3-dependent ubiquitination of ASC. FASEB J 33:8865–8877. https://doi.org/10.1096/fj.201802418R.
21. Santoro MG, Rossi A, Amici C. 2003. NF-kappaB and virus infection: who controls whom. EMBO J 22:2552–2560. https://doi.org/10.1093/emboj/cdg267.
22. Kern DM, Sorum B, Mali SS, Hoel CM, Sridharan S, Remis JP, Toso DB, Kotecha A, Bautista DM, Brohawn SG. 2021. Cryo-EM structure of SARS-CoV-2 ORF3a in lipid nanodiscs. Nat Struct Mol Biol 28:573–582. https://doi.org/10.1038/s41594-021-00619-0.
23. Andrews N, Tessier E, Stowe J, Gower C, Kirsebom F, Simmons R, Gallagher E, Thelwall S, Groves N, Dabrera G, Myers R, Campbell CNJ, Amirthalingam G, Edmunds M, Zambon M, Brown K, Hopkins S, Chand M, Ladhani SN, Ramsay M, Lopez Bernal J. 2022. Duration of protection against mild and severe disease by Covid-19 vaccines. N Engl J Med 386:340–350. https://doi.org/10.1056/NEJMoa2115481.
24. Painter WP, Holman W, Bush JA, Almazedi F, Malik H, Eraut NCJE, Morin MJ, Szewczyk LJ, Painter GR. 2021. Human safety, tolerability, and pharmacokinetics of molnupiravir, a novel broad-spectrum oral antiviral agent with activity against SARS-CoV-2. Antimicrob Agents Chemother 65:e02428-20. https://doi.org/10.1128/AAC.02428-20.
25. Vuong W, Khan MB, Fischer C, Arutyunova E, Lamer T, Shields J, Saffran HA, McKay RT, van Belkum MJ, Joyce MA, Young HS, Tyrrell DL, Vederas JC, Lemieux MJ. 2020. Feline coronavirus drug inhibits the main protease of SARS-CoV-2 and blocks virus replication. Nat Commun 11:4282. https://doi.org/10.1038/s41467-020-18096-2.
26. Naqvi AAT, Fatima K, Mohammad T, Fatima U, Singh IK, Singh A, Atif SM, Hariprasad G, Hasan GM, Hassan MI. 2020. Insights into SARS-CoV-2 genome, structure, evolution, pathogenesis and therapies: structural genomics approach. Biochim Biophys Acta Mol Basis Dis 1866:165878. https://doi.org/10.1016/j.bbadis.2020.165878.
27. Potempa M, Lee SK, Wolfenden R, Swanstrom R. 2015. The triple threat of HIV-1 protease inhibitors. Curr Top Microbiol Immunol 389:203–241. https://doi.org/10.1007/82_2015_438.
28. De Luca A, Bianco C, Rossetti B. 2014. Treatment of HCV infection with the novel NS3/4A protease inhibitors. Curr Opin Pharmacol 18:9–17. https://doi.org/10.1016/j.coph.2014.07.016.
29. Mahdi M, Mótyán JA, Szojka ZI, Golda M, Miczi M, Tőzsér J. 2020. Analysis of the efficacy of HIV protease inhibitors against SARS-CoV-2's main protease. Virol J 17:190. https://doi.org/10.1186/s12985-020-01457-0.
30. Bafna K, White K, Harish B, Rosales R, Ramelot TA, Acton TB, Moreno E, Kehrer T, Miorin L, Royer CA, García-Sastre A, Krug RM, Montelione GT. 2021. Hepatitis C virus drugs that inhibit SARS-CoV-2 papain-like protease synergize with remdesivir to suppress viral replication in cell culture. Cell Rep 35:109133. https://doi.org/10.1016/j.celrep.2021.109133.
31. Macchiagodena M, Pagliai M, Procacci P. 2022. Characterization of the non-covalent interaction between the PF-07321332 inhibitor and the SARS-CoV-2 main protease. J Mol Graph Model 110:108042. https://doi.org/10.1016/j.jmgm.2021.108042.
32. Keum YS, Jeong YJ. 2012. Development of chemical inhibitors of the SARS coronavirus: viral helicase as a potential target. Biochem Pharmacol 84:1351–1358. https://doi.org/10.1016/j.bcp.2012.08.012.
33. Knoops K, Kikkert M, Worm S. H E v d, Zevenhoven-Dobbe JC, van der Meer Y, Koster AJ, Mommaas AM, Snijder EJ. 2008. SARS-coronavirus replication is supported by a reticulovesicular network of modified endoplasmic reticulum. PLoS Biol 6:e226. https://doi.org/10.1371/journal.pbio.0060226.
34. Brant AC, Tian W, Majerciak V, Yang W, Zheng ZM. 2021. SARS-CoV-2: from its discovery to genome structure, transcription, and replication. Cell Biosci 11:136. https://doi.org/10.1186/s13578-021-00643-z.
35. Wolff G, Melia CE, Snijder EJ, Barcena M. 2020. Double-membrane vesicles as platforms for viral replication. Trends Microbiol 28:1022–1033. https://doi.org/10.1016/j.tim.2020.05.009.
36. Hagemeijer MC, Monastyrska I, Griffith J, van der Sluijs P, Voortman J, van Bergen En Henegouwen PM, Vonk AM, Rottier PJM, Reggiori F, de Haan CAM. 2014. Membrane rearrangements mediated by coronavirus nonstructural proteins 3 and 4. Virology 458–459:125–135. https://doi.org/10.1016/j.virol.2014.04.027.
37. McClenaghan C, Hanson A, Lee SJ, Nichols CG. 2020. Coronavirus proteins as ion channels: current and potential research. Front Immunol 11:573339. https://doi.org/10.3389/fimmu.2020.573339.
38. Chen D, Zheng Q, Sun L, Ji M, Li Y, Deng H, Zhang H. 2021. ORF3a of SARS-CoV-2 promotes lysosomal exocytosis-mediated viral egress. Dev Cell 56:3250–3263.e5. https://doi.org/10.1016/j.devcel.2021.10.006.
39. Nagy Á, Pongor S, Győrffy B. 2021. Different mutations in SARS-CoV-2 associate with severe and mild outcome. Int J Antimicrob Agents 57:106272. https://doi.org/10.1016/j.ijantimicag.2020.106272.
40. Issa E, Merhi G, Panossian B, Salloum T, Tokajian S. 2020. SARS-CoV-2 and ORF3a: nonsynonymous mutations, functional domains, and viral pathogenesis. mSystems 5:e00266-20. https://doi.org/10.1128/mSystems.00266-20.
41. Zhang J, Wu H, Yao X, Zhang D, Zhou Y, Fu B, Wang W, Li H, Wang Z, Hu Z, Ren Y, Sun R, Tian Z, Bian X, Wei H. 2021. Pyroptotic macrophages stimulate the SARS-CoV-2-associated cytokine storm. Cell Mol Immunol 18:1305–1307. https://doi.org/10.1038/s41423-021-00665-0.

42. Hachim A, Kavian N, Cohen CA, Chin AWH, Chu DKW, Mok CKP, Tsang OTY, Yeung YC, Perera RAPM, Poon LLM, Peiris JSM, Valkenburg SA. 2020. ORF8 and ORF3b antibodies are accurate serological markers of early and late SARS-CoV-2 infection. Nat Immunol 21:1293–1301. https://doi.org/10.1038/s41590-020-0773-7.
43. Silvas JA, Vasquez DM, Park J-G, Chiem K, Allué-Guardia A, Garcia-Vilanova A, Platt RN, Miorin L, Kehrer T, Cupic A, Gonzalez-Reiche AS, Bakel H. v, García-Sastre A, Anderson T, Torrelles JB, Ye C, Martinez-Sobrido L. 2021. Contribution of SARS-CoV-2 accessory proteins to viral pathogenicity in K18 human ACE2 transgenic mice. J Virol 95:e0040221. https://doi.org/10.1128/JVI.00402-21.
44. Yount B, Roberts RS, Sims AC, Deming D, Frieman MB, Sparks J, Denison MR, Davis N, Baric RS. 2005. Severe acute respiratory syndrome coronavirus group-specific open reading frames encode nonessential functions for replication in cell cultures and mice. J Virol 79:14909–14922. https://doi.org/10.1128/JVI.79.23.14909-14922.2005.
45. Zhang X, Liu Y, Liu J, Bailey AL, Plante KS, Plante JA, Zou J, Xia H, Bopp NE, Aguilar PV, Ren P, Menachery VD, Diamond MS, Weaver SC, Xie X, Shi P-Y. 2021. A trans-complementation system for SARS-CoV-2 recapitulates authentic viral replication without virulence. Cell 184:2229–2238.e2213. https://doi.org/10.1016/j.cell.2021.02.044.
46. Rice AP, Kimata JT. 2021. SARS-CoV-2 likely targets cellular PDZ proteins: a common tactic of pathogenic viruses. Future Virol https://doi.org/10.2217/fvl-2020-0365.
47. Ren Y, Shu T, Wu D, Mu J, Wang C, Huang M, Han Y, Zhang X-Y, Zhou W, Qiu Y, Zhou X. 2020. The ORF3a protein of SARS-CoV-2 induces apoptosis in cells. Cell Mol Immunol 17:881–883. https://doi.org/10.1038/s41423-020-0485-9.
48. Fernandes IG, de Brito CA, Dos Reis VMS, Sato MN, Pereira NZ. 2020. SARS-CoV-2 and other respiratory viruses: what does oxidative stress have to do with it? Oxid Med Cell Longev 2020:8844280. https://doi.org/10.1155/2020/8844280.
49. Li Z, Xu X, Leng X, He M, Wang J, Cheng S, Wu H. 2017. Roles of reactive oxygen species in cell signaling pathways and immune responses to viral infections. Arch Virol 162:603–610. https://doi.org/10.1007/s00705-016-3130-2.
50. Holze C, Michaudel C, Mackowiak C, Haas DA, Benda C, Hubel P, Pennemann FL, Schnepf D, Wettmarshausen J, Braun M, Leung DW, Amarasinghe GK, Perocchi F, Staeheli P, Ryffel B, Pichlmair A. 2018. Oxeiptosis, a ROS-induced caspase-independent apoptosis-like cell-death pathway. Nat Immunol 19:130–140. https://doi.org/10.1038/s41590-017-0013-y.
51. Sayah W, Berkane I, Guermache I, Sabri M, Lakhal FZ, Yasmine Rahali S, Djidjeli A, Lamara Mahammed L, Merah F, Belaid B, Berkani L, Lazli NZ, Kheddouci L, Kadi A, Ouali M, Khellafi R, Mekideche D, Kheliouen A, Hamidi RM, Ayoub S, Raaf NB, Derrar F, Gharnaout M, Allam I, Djidjik R. 2021. Interleukin-6, procalcitonin and neutrophil-to-lymphocyte ratio: potential immune-inflammatory parameters to identify severe and fatal forms of COVID-19. Cytokine 141:155428. https://doi.org/10.1016/j.cyto.2021.155428.
52. Del Valle DM, Kim-Schulze S, Huang H-H, Beckmann ND, Nirenberg S, Wang B, Lavin Y, Swartz TH, Madduri D, Stock A, Marron TU, Xie H, Patel M, Tuballes K, Van Oekelen O, Rahman A, Kovatch P, Aberg JA, Schadt E, Jagannath S, Mazumdar M, Charney AW, Firpo-Betancourt A, Mendu DR, Jhang J, Reich D, Sigel K, Cordon-Cardo C, Feldmann M, Parekh S, Merad M, Gnjatic S. 2020. An inflammatory cytokine signature predicts COVID-19 severity and survival. Nat Med 26:1636–1643. https://doi.org/10.1038/s41591-020-1051-9.
53. Aboudounya MM, Heads RJ. 2021. COVID-19 and Toll-like receptor 4 (TLR4): SARS-CoV-2 may bind and activate TLR4 to increase ACE2 expression, facilitating entry and causing hyperinflammation. Mediators Inflamm 2021:8874339. https://doi.org/10.1155/2021/8874339.
54. Matsumoto M, Funami K, Tatematsu M, Azuma M, Seya T. 2014. Assessment of the Toll-like receptor 3 pathway in endosomal signaling. Methods Enzymol 535:149–165. https://doi.org/10.1016/B978-0-12-397925-4.00010-9.
55. Brandao SCS, Ramos JOX, Dompieri LT, Godoi ETAM, Figueiredo JL, Sarinho ESC, Chelvanambi S, Aikawa M. 2021. Is Toll-like receptor 4 involved in the severity of COVID-19 pathology in patients with cardiometabolic comorbidities? Cytokine Growth Factor Rev 58:102–110. https://doi.org/10.1016/j.cytogfr.2020.09.002.
56. Mukherjee R, Bhattacharya A, Bojkova D, Mehdipour AR, Shin D, Khan KS, Hei-Yin Cheung H, Wong K-B, Ng W-L, Cinatl J, Geurink PP, van der Heden van Noort GJ, Rajalingam K, Ciesek S, Hummer G, Dikic I. 2021. Famotidine inhibits toll-like receptor 3-mediated inflammatory signaling in SARS-CoV-2 infection. J Biol Chem 297:100925. https://doi.org/10.1016/j.jbc.2021.100925.
57. Mather JF, Seip RL, McKay RG. 2020. Impact of famotidine use on clinical outcomes of hospitalized patients with COVID-19. Am J Gastroenterol 115:1617–1623. https://doi.org/10.14309/ajg.0000000000000832.
58. Beltran-Garcia J, Osca-Verdegal R, Pallardó FV, Ferreres J, Rodríguez M, Mulet S, Sanchis-Gomar F, Carbonell N, García-Giménez JL. 2020. Oxidative stress and inflammation in COVID-19-associated sepsis: the potential role of anti-oxidant therapy in avoiding disease progression. Antioxidants (Basel) 9:936. https://doi.org/10.3390/antiox9100936.
59. Yang S, Tian M, Johnson AN. 2020. SARS-CoV-2 protein ORF3a is pathogenic in Drosophila and causes phenotypes associated with COVID-19 post-viral syndrome. bioRxiv https://doi.org/10.1101/2020.12.20.423533.
60. Gaddy DF, Lyles DS. 2005. Vesicular stomatitis viruses expressing wild-type or mutant M proteins activate apoptosis through distinct pathways. J Virol 79:4170–4179. https://doi.org/10.1128/JVI.79.7.4170-4179.2005.
61. Caillet-Saguy C, Durbesson F, Rezelj VV, Gogl G, Tran QD, Twizere JC, Vignuzzi M, Vincentelli R, Wolff N. 2021. Host PDZ-containing proteins targeted by SARS-CoV-2. FEBS J 288:5148–5162. https://doi.org/10.1111/febs.15881.
62. Majumdar P, Niyogi S. 2020. ORF3a mutation associated with higher mortality rate in SARS-CoV-2 infection. Epidemiol Infect 148:e262. https://doi.org/10.1017/S0950268820002599.
63. Wang R, Chen J, Gao K, Hozumi Y, Yin C, Wei G-W. 2021. Analysis of SARS-CoV-2 mutations in the United States suggests presence of four substrains and novel variants. Commun Biol 4:228. https://doi.org/10.1038/s42003-021-01754-6.
64. Chu DKW, Hui KPY, Gu H, Ko RLW, Krishnan P, Ng DYM, Liu GYZ, Wan CKC, Cheung M-C, Ng K-C, Nicholls JM, Tsang DNC, Peiris M, Chan MCW, Poon LLM. 2021. Introduction of ORF3a-Q57H SARS-CoV-2 variant causing fourth epidemic wave of COVID-19, Hong Kong, China. Emerg Infect Dis 27:1492–1495. https://doi.org/10.3201/eid2705.210015.
65. Wu S, Tian C, Liu P, Guo D, Zheng W, Huang X, Zhang Y, Liu L. 2021. Effects of SARS-CoV-2 mutations on protein structures and intraviral protein-protein interactions. J Med Virol 93:2132–2140. https://doi.org/10.1002/jmv.26597.
66. Nkeze J, Li L, Benko Z, Li G, Zhao RY. 2015. Molecular characterization of HIV-1 genome in fission yeast *Schizosaccharomyces pombe*. Cell Biosci 5:47. https://doi.org/10.1186/s13578-015-0037-7.
67. Huard S, Chen M, Burdette KE, Fenyvuesvolgyi C, Yu M, Elder RT, Zhao RY. 2008. HIV-1 Vpr-induced cell death in *Schizosaccharomyces pombe* is reminiscent of apoptosis. Cell Res 18:961–973. https://doi.org/10.1038/cr.2008.272.
68. Zhao RY, Liang D, Li G, Larrimore CW, Mirkin BL. 2010. Anti-cancer effect of HIV-1 viral protein R on doxorubicin resistant neuroblastoma. PLoS One 5:e11466. https://doi.org/10.1371/journal.pone.0011466.
69. Li G, Makar T, Gerzanich V, Kalakonda S, Ivanova S, Pereira EFR, Andharvarapu S, Zhang J, Simard JM, Zhao RY. 2020. HIV-1 Vpr-induced proinflammatory response and apoptosis are mediated through the Sur1-Trpm4 channel in astrocytes. mBio 11:e02939-20. https://doi.org/10.1128/mBio.02939-20.
70. Harcourt J, Tamin A, Lu X, Kamili S, Sakthivel SK, Murray J, Queen K, Tao Y, Paden CR, Zhang J, Li Y, Uehara A, Wang H, Goldsmith C, Bullock HA, Wang L, Whitaker B, Lynch B, Gautam R, Schindewolf C, Lokugamage KG, Scharton D, Plante JA, Mirchandani D, Widen SG, Narayanan K, Makino S, Ksiazek TG, Plante KS, Weaver SC, Lindstrom S, Tong S, Menachery VD, Thornburg NJ. 2020. Severe acute respiratory syndrome coronavirus 2 from patient with 2019 novel coronavirus disease, United States. Emerg Infect Dis 26:1266–1273. https://doi.org/10.3201/eid2606.200516.